# Fragmentation of atomic clusters: A theoretical study

Maria J. López* and Julius Jellinek
*Chemistry Division, Argonne National Laboratory, Argonne, Illinois 60439*
(Received 8 November 1993)

Collisionless fragmentation of nonrotating model $n$-atom metal clusters ($n=12$, 13, and 14) is studied using isoergic molecular-dynamics simulations. Minimum-energy paths for fragmentation are mapped out as functions of the distance between the centers of mass of the fragments. These paths provide information on the fragmentation energies for the different fragmentation channels. Fragmentation patterns (distributions of the fragmentation channel probabilities) and global and channel-specific fragmentation rate constants are computed and analyzed as functions of the internal energy and of the size of the clusters. The trends derived from the dynamics are compared with those obtained using the RRK and TST statistical approaches. The dynamics of the fragmentation process is analyzed in terms of characteristic quantities such as the distance between the centers of mass of the fragments, their relative translational energy, and their interaction energy, all considered as functions of time.

PACS number(s): 36.40.+d

## I. INTRODUCTION

Fragmentation, or dissociation, of energized clusters (including the ejection of a single atom, i.e., evaporation, as a particular case) is a process common to many cluster experiments [1–9]. In some cases fragmentation is an undesirable phenomenon that complicates the interpretation of the experimental data [2]. In others [3–9] it is taken advantage of to make inferences about the relative stability of clusters, the binding energies, and the flow and redistribution (localization) of the energy in a cluster.

One of the parameters affecting the time scale of cluster fragmentation is the excess energy, i.e., the energy above the fragmentation barrier. In cases with no fragmentation barrier, the excess energy is that above the minimum energy of the separated fragments. Upon fragmentation, the excess energy is partitioned among the internal (vibrational), rotational, and translational degrees of freedom of the fragments. Lifetimes of the clusters, kinetic-energy release distributions, and information on binding energies can be extracted from data obtained in collision-induced dissociation [3,4,9] and photodissociation [5–8] experiments. The knowledge of these can then be combined with statistical theories [10–15] of unimolecular decay of energized species to arrive at estimates of the fragmentation energies. The accuracy of these estimates, however, is limited because the distribution of the internal energy of the clusters usually is not known and the values of most of the parameters used in the statistical models are known only approximately. Even if one were able to correct for these shortcomings, the statistical theories would still provide no information on the dynamics (mechanisms) of the fragmentation process. Such information can be obtained from molecular-dynamics (MD) simulations. These simulations can also be used to test the validity of the statistical models [16,17].

Molecular-dynamics simulations [16–33] have been utilized extensively to investigate a wide variety of structural and dynamical properties of clusters, which include their isomers and isomerization transitions, phases (e.g., solidlike and liquidlike) and phase changes (e.g., a meltinglike transition), etc. These simulations were carried out for systems with van der Waals [16–21], covalent [22], ionic [23–25], and metallic [26–33] cohesion. In contrast, the fragmentation of clusters has been the subject only of a limited number of MD studies, almost all of which considered Lennard-Jones systems [16,17,33–37]. Evaporation (ejection of single atoms) emerged in these studies as the only dissociation channel. No dynamical description of a possible multichannel fragmentation has yet been given. Experiments on metal cluster ions [5], however, furnish evidence for such a phenomenon. Multichannel fragmentation of atomic nuclei has been studied extensively using statistical theories [38,39]. Limited application of these theories to clusters has also been considered [16,17,40,41]. However, the phenomenon of cluster fragmentation, in general, and the dynamics (mechanisms) characterizing it, in particular, remain largely a *terra incognita*.

In this paper we present results of a MD study of the collisionless fragmentation of model $(M)_n$ [$(M)$ stands for "metal"] clusters,

$$(M)_n \rightarrow (M)_i + (M)_{n-i} , \tag{1}$$

where $n=12,13,14$ and $i\,(\leq n/2)$ is the size of the smaller fragment. For a given $n$, $i$ labels the different fragmentation channels. (The reader will easily make a distinction between this and an alternative use of $i$ as a label of the individual atoms.) An intriguing finding is that, in contrast to Lennard-Jones systems [16,17,34–37], the model $(M)_n$ clusters mimicked by a potential specified

*On leave of absence from Departamento de Física Teórica, Facultad de Ciencias, Universidad de Valladolid, Valladolid, Spain.

 

below, fragment preferentially into products larger than monomers. In fact, evaporation of monomers appears to be the least probable channel. (For a discussion of the robustness of this finding, see Sec. IV.) The fragmentation patterns of the clusters and their dissociation rate constants (global and channel-specific) are calculated as functions of the cluster energy and size. The dynamics of the cluster fragmentation is analyzed by monitoring the short-time-averaged internal kinetic energy of the $n$-atom system, the relative kinetic energy and the interaction energy of the fragments, and the separation between the centers of mass (c.o.m.'s) of the fragments, all considered as functions of time.

Obviously, the dynamics and the outcome of the fragmentation process depend on the potential describing the interaction between the atoms in the cluster. The semiempirical potentials used in numerical simulations are usually fitted to measured properties, at least some of which may be (and in most cases indeed are) size dependent. Therefore, in the case of clusters, the validity of these potentials is, in principle, limited to a certain cluster size or sizes. It has been suggested [30] to incorporate explicitly the size dependence into semiempirical interaction potentials in order to achieve a higher degree of their flexibility and, consequently, adequacy. Since the fragmentation phenomenon by its very nature implies simultaneous consideration of systems (clusters) of disparate sizes, it constitutes an especially difficult test for a fitted potential. In practice, the properties of the bulk and, less often, also of the diatomic molecule of an element are used most frequently to fit the parameters of a potential since experimental data for these are most readily available.

The emphasis of this study is on the analysis of the dynamics of the fragmentation process as defined by the potential chosen to mimic a cluster. The results are then compared with predictions of statistical models. We employ a semiempirical Gupta-like potential [26,30] that incorporates many-body effects known to play an important role in metallic cohesion. The details of the potential, the computational procedure, and the theoretical background are discussed in Secs. II and III. The numerical results and their analysis are given in Sec. IV. We conclude with a brief summary.

## II. THEORETICAL BACKGROUND AND COMPUTATIONAL PROCEDURE

The goal of this study is to analyze structural, energetic, and dynamical aspects of the process of fragmentation of clusters as defined by their size and total energy. The clusters are mimicked by an $n$-body potential that is based on Gupta's expression [42] for the cohesive energy of bulk metals. The attractive part of the interatomic interaction is based on the second moment approximation to the tight-binding model. It is this part that incorporates all the $n(>2)$-body effects. The repulsive part is a sum of pairwise Born-Mayer terms. In reduced units of energy $V^*$ and interatomic distances $r_{ij}^*$ the potential is written as [26,30]

$$V^*=\frac{1}{2}\sum_{j=1}^{n}\left\{A\sum_{i(\neq j)=1}^{n}\exp[-p(r_{ij}^*-1)]-\left[\sum_{i(\neq j)=1}^{n}\exp[-2q(r_{ij}^*-1)]\right]^{1/2}\right\}, \tag{2}$$

where the parameters $A$, $p$, and $q$ depend on the material (element). We adopt the values $p=9$ and $q=3$, which have been used for transition metals [43]. The reduced energy $V^*$ and distance $r_{ij}^*$ are defined as

$$V^*=\frac{V}{U}\ , \quad r_{ij}^*=\frac{r_{ij}}{r_0}\ , \tag{3}$$

where $V$ and $r_{ij}$ are the corresponding values of the energy and distance in absolute units, $r_0$ is the equilibrium nearest-neighbor distance of the bulk metal in absolute units, and $U$ plays the role of a unit of energy. The value $A=0.101\,036$ is obtained by maximizing the (converged) cohesive energy of an fcc metal at the equilibrium value of its nearest-neighbor distance.

Introducing the reduced time $t^*=t/t_0$, where the unit $t_0$ of time $t$ is defined by

$$t_0=r_0\sqrt{m/U}\ , \tag{4}$$

one obtains the classical equations of motion for the atoms of the system in the form

$$\frac{d^2\mathbf{r}_i^*}{dt^{*2}}=-\frac{\partial V^*}{\partial \mathbf{r}_i^*}\ , \quad i=1,\ldots,n\ , \tag{5}$$

where $\mathbf{r}_i^*$ is the position vector of atom $i$ in reduced units. In Eq. (4), $m$ stands for the mass of an atom. It is implied in Eqs. (5) that the mass of an atom in reduced units $m^*$ is equal to 1. Equations (5) eliminate the explicit dependence on $U$, which means that the qualitative features of the dynamics defined by the Gupta-like potential, Eq. (2), are $U$ independent. Equations (5) are solved using the velocity version of the Verlet algorithm [44]. The initial coordinates and momenta of the atoms in the cluster are chosen to yield zero total linear and angular momenta. The time step of $\Delta t^*=10^{-2}$ assures conservation of the total energy even in the longest runs ($10^7$ steps) well within 0.01%.

The quantities we use to characterize the fragmentation of a cluster of a specified size and total energy include the following.

(1) Channel fragmentation energy $E_0(i)$, which is defined as the height of the barrier ("transition state") along the minimum-energy path connecting the configuration space of the parent cluster to that of the fragments of the channel $i$. In case such a barrier is absent, $E_0(i)$ is the difference between the energy of the most stable structure of the parent cluster and the sum of the energies of the most stable structures of the fragments. This latter case is the one of the so-called loose transition state. Classically, the fragmentation energy is the threshold value of the internal energy below which the cluster never fragments and above which it fragments with probability 1. (Exceptions are those cases when the motion of the cluster is trapped in the plane orthogonal to the fragmentation path.) One should note, however,

that even at energies substantially higher than the fragmentation energy one may have to wait a very long time to actually observe the fragmentation of the cluster.

(2) Fragmentation-channel probability $\mathcal{P}_i$,

$$\mathcal{P}_i=\frac{N_{i0}}{N_0} , \tag{6}$$

where $N_0$ is the total number of clusters considered for a fixed total energy and size and $N_{i0}$ is the number of these clusters that fragment into channel $i$. In simulations we use the definition

$$\mathcal{P}_i=\frac{\tilde{N}_{i0}}{\tilde{N}_0} , \tag{6'}$$

where $\tilde{N}_0$ is the total number of simulation runs (trajectories) that lead to fragmentation of the cluster within a specified interval of time ("observation time"), and $\tilde{N}_{i0}$ is the number of these trajectories that result in fragmentation into channel $i$:

$$\tilde{N}_0=\sum_i \tilde{N}_{i0} . \tag{7}$$

The reason for introducing an observation time in numerical simulations is the fact mentioned above that certain initial conditions may lead to prohibitively long survival of the cluster. In our study the length of the observation time interval is $10^7$ steps. Of course, the definitions (6) and (6') are equivalent only if the probabilities $\mathcal{P}_i$ are time independent (see below).

(3) Interaction energy $E_{\rm int}$ defined as

$$E_{\rm int}(t)=V_n(t)-[V_i(t)+V_{n-i}(t)] , \tag{8}$$

where $V_n(t)$, $V_i(t)$, and $V_{n-i}(t)$ are the potential energies of the $n$-, $i$-, and $(n-i)$-atom systems, respectively. Before the fragmentation, the $n$ atoms form the parent cluster. The $i$- and $(n-i)$-atom systems are the ones that become the fragments of the dissociated cluster. In order to follow the time evolution of $E_{\rm int}$ along a phase-space trajectory corresponding to the fragmentation of the cluster, one has to know both the fragmentation channel $i$ and the identity of the atoms (specified by their numerical label) in each of the fragments. Of course, the fragments and the identity of the atoms in them are known only after the breakup of the cluster. The test for fragmentation involves monitoring the interatomic distances and identifying $i$- and $(n-i)$-atom systems such that the atoms within these systems remain bounded, as judged by the corresponding interatomic distances, whereas the separation between the atoms belonging to different systems becomes arbitrarily large. In order to calculate $E_{\rm int}(t)$, as well as other time-dependent quantities that presume knowledge of the identity of the fragments before the actual fragmentation of the cluster takes place, one must recompute the trajectory, or at least a part of it. It is clear from definition (8) that $E_{\rm int}\to 0$ as the cluster fragments.

(4) Kinetic energy of the relative motion of the fragments ("kinetic-energy release") $E_{k\rm rel}$,

$$E_{k\rm rel}(t)=\frac{\mathbf{P}_i^2(t)}{2M_i}+\frac{\mathbf{P}_{n-i}^2(t)}{2M_{n-i}}=\frac{1}{2\mu}P^2(t) , \tag{9}$$

where $\mathbf{P}_i$ and $\mathbf{P}_{n-i}$ are the total linear momenta of the $i$- and $(n-i)$-atom fragments, respectively, measured with respect to the c.o.m. of the $n$-atom system ($\mathbf{P}_i=-\mathbf{P}_{n-i}$), $M_i$ and $M_{n-i}$ are the masses of the fragments, $P=P_i=P_{n-i}$, and $\mu=M_iM_{n-i}/(M_i+M_{n-i})$ is the reduced mass of the fragments.

(5) Time-dependent survival probability $\mathcal{P}(t)$,

$$\mathcal{P}(t)=\frac{1}{N_0}\sum_{i=1}^{N_0}\theta(\tau_{0i}-t) , \tag{10}$$

where $\theta$ is the Heaviside step function, $\tau_{0i}$ is the survival time of the cluster, i.e., the time the cluster lives before it undergoes fragmentation, along the trajectory $i$, and $N_0(\geq\tilde{N}_0)$ is the same as in Eq. (6). (The definition of the instant of fragmentation is given below.)

(6) Global fragmentation rate constant $k$ defined by the equation

$$\frac{dN(t)}{dt}=-kN(t) , \tag{11}$$

where $N(t)$ is the number of surviving parent clusters at time $t$ [$N(t=0)=N_0$]. Assuming that $k$ does not depend on time, Eq. (11) implies the relation

$$\mathcal{P}(t)=e^{-kt} , \tag{12}$$

which allows one to calculate $k$ by fitting $\ln[\mathcal{P}(t)]$ to a linear function. Since $\mathcal{P}(t)$ depends parametrically on the total energy of the cluster, $k$ is a function of this energy, i.e., it is the microcanonical rate constant.

(7) Channel-specific (time-independent) rate constant $k_i$ defined by the equation

$$\frac{dN_i(t)}{dt}=-k_iN(t) , \tag{13}$$

where $N_i(t)$ is the number of surviving parent clusters at time $t$ that are destined to fragment into channel $i$. Summing both sides of Eq. (13) over $i$, taking into account that $\sum_i N_i(t)=N(t)$, and comparing with Eq. (11), one arrives at

$$k=\sum_i k_i . \tag{14}$$

Another relation between the rate constants can be obtained by combining Eqs. (11) and (13):

$$\frac{d}{dt}[kN_i(t)-k_iN(t)]=0 , \tag{15}$$

i.e.,

$$kN_i(t)-k_iN(t)=C . \tag{16}$$

Taking into account that $N_i(t=\infty)=0$ and $N(t=\infty)=0$, one obtains $C=0$. Incorporating Eq. (6) into Eq. (16) evaluated at $t=0$, we arrive then at

$$k_i=\mathcal{P}_ik . \tag{17}$$

Substitution of Eq. (17) into Eq. (16) leads to

$$\mathcal{P}_i(t)=\mathcal{P}_i \ , \tag{18}$$

where $\mathcal{P}_i(t)=N_i(t)/N(t)$ and $\mathcal{P}_i=\mathcal{P}_i(t=0)$ is defined by Eq. (6). This proves that the fragmentation-channel probabilities are time independent.

In order to analyze the energy dependence of the fragmentation of clusters we have computed the probabilities and rate constants at different values of the internal (alternatively, total) energy. The initial conditions for trajectories corresponding to a chosen energy were generated from phase-space coordinates recorded along a trajectory at energy lower than the desired one by 0.05–0.5 %. The coordinates were recorded every 5000th propagation step, which was adequate for losing the "memory" of the trajectory. The momenta of the atoms were scaled to arrive at the desired total energy of the cluster. The adequacy of sampling of the relevant part of the energy shell with a set of initial conditions generated in this way was tested by generating another set of initial conditions for the same energy from phase-space coordinates recorded along a trajectory at energy lower by 5%. Within the statistical error, the two sets of initial conditions produced identical results. The convergence of the results was tested by varying the number of the initial conditions at fixed values of the total energy (see Sec. IV).

## III. STATISTICAL MODELS

An alternative to the dynamical analyses is the use of statistical models [10–15]. In fact, these models have been favored as the approach of choice in studies of unimolecular, i.e., collisionless, processes, including fragmentation. The basic assumptions of the statistical models are that (1) global (as opposed to detailed) features of physical processes are defined primarily by the energetic characteristics of the system, and (2) the energy available to the system is randomized rapidly between its active (i.e., coupled to the relevant for the process of interest) degrees of freedom.

The simplest statistical approach to unimolecular processes is the RRK [10,12,13] (Rice-Ramsperger-Kassel) model, which assumes that all the degrees of freedom of the system are vibrational and all are strongly coupled. It states that the system undergoes a unimolecular process (e.g., an isomerization or a fragmentation into a specified channel) when and if the energy localized in a specified vibrational degree of freedom becomes equal or larger than a certain threshold value ($E_0$). The rate constant $k(E)$ of the process is proportional to the probability of such a localization and is given by [12]

$$k(E)=\nu\left[1-\frac{E_0}{E}\right]^{s-1} \ , \tag{19}$$

where $E \geq E_0$ is the total energy of the system, $s$ is the number of its degrees of freedom, and $\nu$ is a frequency proportionality constant.

A more elaborate approach is the transition-state theory (TST) (for a review see, e.g., Ref. [45]), which for unimolecular processes is known as the RRKM (RRK-Marcus) scheme [11–13]. The TST approach introduces a "transition state of the system," which is defined as a $(6n-1)$-dimensional dividing surface separating the "reactant(s)" and the "product(s)" parts of the phase space. (The conservation laws reduce the dimensionality of the relevant parts of the phase space and of the transition state.) The "reaction" takes place when and if the phase point of the system, moving along a one-dimensional manifold called the reaction path, crosses the transition state. The rate of the reaction is defined as the rate of reaching or, what is assumed to be equivalent, crossing the transition state by the phase points originating in the reactants part of the phase space. The TST expression for the microcanonical rate constant $k(E,J)$ is [12]

$$k(E,J)=\frac{1}{h}\frac{W^{\dagger}(E,J)}{\rho(E,J)} \ , \tag{20}$$

where $W^{\dagger}(E,J)$ is the total number of microstates in the transition state accessible to the system with the total energy $E$ and magnitude $J$ of the total angular momentum, $\rho(E,J)$ is the density of states of the system in the reactants part of its phase space, and $h$ is Planck's constant.

One of the complex issues of the TST theory is the choice of the transition state [45]. This choice is especially problematic in cases when the reaction paths do not possess a barrier and one has to deal with so-called loose transition states (for a discussion see, e.g., Refs. [13,15]. As is shown in Sec. IV, the fragmentation of the model clusters considered here is, in fact, such a case. We select the distance between the c.o.m.'s of the fragments as the reaction coordinate and place the transition state at that value of this coordinate at which the fragments become free, i.e., their interaction energy, calculated from configurations generating the minimum-energy path (see Sec. IV), becomes zero. More precisely, we consider the fragments as free when the absolute value of their interaction energy becomes smaller than a predefined small positive quantity. This implies that the transition state corresponds to a finite separation between the fragments. The calculation of the total number of microstates $W^{\dagger}(E,J)$ is based on the scheme described recently by Smith [14]. This scheme incorporates the orbital and rotational motions of the fragments compatible with the fixed total energy and magnitude of the total angular momentum of the system of $n$ atoms. The derivations and details will be given elsewhere. Here we present the result only for the case of nonrotating parent clusters and channel $i=2$, which is of primary relevance for the model potential considered in this study (see Sec. IV):

$$W^{\dagger}(E,J=0)=\frac{n!}{\sigma_1\sigma_2}\frac{\pi}{\hbar^4}\frac{I_1^{3/2}I_2^{1/2}I_0^{1/2}}{(I_1+I_2+I_0)^{1/2}}\frac{1}{\prod_{i=1}^{s-5}\hbar\nu_i^{\dagger}}\frac{2}{(s-3)!} \times[E-E_0(2)]^{s-3} \ . \tag{21}$$

Equation (21) is obtained under the following conditions. The transition state of the system is comprised of a dimer and an $(n-2)$-atom fragment, assumed to be a spherical top, which do not interact. The internal vibrations in the fragments are assumed to be harmonic and decoupled from the rotational and orbital motions of the fragments.

In describing the orbital motion, the two fragments are treated as point masses. In Eq. (21), $I_1$ is the moment of inertia of the spherical top [$(n-2)$-atom fragment], $I_2$ is the doubly degenerate moment of inertia of the dimer, and $I_0$ is the doubly degenerate moment of inertia of the two point-mass fragments. $I_0$, $I_1$, and $I_2$ are defined, respectively, in the principal axes frames corresponding to these three systems. $\sigma_1$ and $\sigma_2$ are the symmetry numbers of the $(n-2)$- and 2-atom fragments, respectively, $s=3n-6$, $\nu_i^\dagger$ $(i=1,\ldots,s-5)$ are the vibrational frequencies of the fragments, $E_0(2)$ is the fragmentation energy of the channel $i=2$, and $\hbar=h/2\pi$. The harmonic density of states $\rho(E,J=0)$ of the nonrotating parent cluster is given by [12]

$$\rho(E,J=0)=\frac{n!}{\sigma}\frac{1}{\prod_{i=1}^{s}\hbar\nu_i}\frac{1}{(s-1)!}E^{s-1}, \tag{22}$$

where $\sigma$ is the symmetry number of the parent cluster and $\nu_i$ $(i=1,\ldots,s)$ are its vibrational frequencies. The $n!$ in Eqs. (21) and (22) is a consequence of considering the atoms distinguishable, as is customary in classical treatments. Note, however, that the rate constant $k(E,J)$, Eq. (20), does not depend on whether the atoms are viewed as distinguishable or indistinguishable.

As is well known [12,13], for unimolecular reactions the TST equation (20) reduces to the RRK equation (19) with

$$\nu=\frac{\prod_{i=1}^{s}\nu_i}{\prod_{i=1}^{s-1}\nu_i^\dagger} \tag{23}$$

when $J=0$ and all the degrees of freedom of the reactant and of the transition state are harmonic vibrations. This suggests identifying the frequency factor $\nu$ of the RRK model as a characteristic frequency of the system.

## IV. RESULTS AND DISCUSSION

Fragmentation of a cluster, as any dynamical process, depends on the topology of the potential-energy surface defining the forces acting on the atoms and on the total energy of the cluster. An important characteristic of the potential-energy surface is the minimum-energy path (MEP) connecting those parts of the configuration space which are of relevance for the dynamical process of interest. The MEP('s) of interest to us is (are) the one(s) which connects the basin(s) of a parent cluster to that (those) of the fragments. The MEP's for fragmentation depend, in principle, on the isomer of the parent cluster and/or of its fragments, and, of course, different MEP's correspond to different fragmentation channels. In fact, a cluster and/or its fragments may undergo isomerization transitions along a minimum-energy path. As a consequence, mapping out the MEP's is a nontrivial problem. An additional difficulty is the computational complexity stemming from the high dimensionality of the potential-energy surface.

We are interested in MEP's because we want to evaluate the fragmentation energy of the clusters. Therefore our goal is to find for each channel the path that connects the point of the configuration space corresponding to the lowest-energy structure of the parent cluster to that of the fragments and which possesses the lowest barrier to the fragmentation. It may turn out that this path has no barrier at all. In cases, when one finds MEP's with nonzero barriers, the search for the lowest barrier may be quite laborious and tedious. On the contrary, finding a single path with no barrier is sufficient to define the fragmentation energy.

It is natural to parameterize the MEP's for fragmentation in terms of the distance $S$ between the centers of mass of the fragments. (The $S$ parametrization may not be adequate in all cases because a MEP may, in principle, contain segments which lie entirely in the subspace orthogonal to $S$.) A way to generate an $S$-parametrized representation of a MEP is to carry out fixed-$S$ constrained minimizations of the energy of the $n$-atom system on a grid of values of $S$. In practice, it is convenient to start with the two fragments in their lowest-energy structure separated by a large $S$ and to perform the constrained energy minimizations on a grid of decreasing values of $S$. Details on mapping out the MEP's, including a discussion of the possible pitfalls and the ways to circumvent them, will be given elsewhere.

Figure 1 illustrates a MEP obtained through $S$-constrained minimizations for the case of fragmentation of a 13-atom cluster into a dimer and an 11-mer. (In this and the subsequent figures we use reduced units, which is indicated by attaching the superscript "*" to the symbols of the physical quantities.) The lowest-lying minimum of the graph (labeled as $I$) corresponds to the most stable icosahedral structure of the 13-atom cluster. The plateau on the right-hand side of the graph (labeled as $V$)

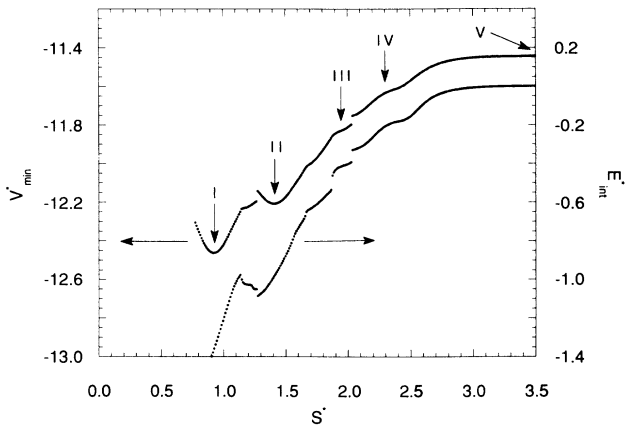


FIG. 1. An $S^*$-parametrized minimum energy path $V^*_{\min}$ and interaction energy $E^*_{\rm int}$ for the fragmentation $(M)_{13}\rightarrow(M)_2+(M)_{11}$. The interaction energy is calculated from the (constrained) minimum-energy configurations corresponding to the minimum-energy path. Five of these configurations labeled by roman numerals are shown in Fig. 2. Here and elsewhere the superscript * means that the quantities are expressed in reduced units.

represents the two free (noninteracting) fragments in their most stable configurations (see Fig. 2). The interaction energy of the fragments calculated from the $S$-constrained minimum-energy configurations of the 13-atom system and of the fragments is shown in Fig. 1 as well. As it should, the interaction energy approaches zero at large separations of the fragments ("large" means $S \geq 3r_0$). One can introduce a definition of "the fragmentation point" along a MEP based on the criterion that the absolute value of the interaction energy becomes less than a predefined small positive quantity. (A definition of "the instant of fragmentation" is given below.) It is clear from Fig. 1 that the fragmentation of the 13-atom cluster into channel $i=2$ takes place without a barrier. We have determined that the same is true for the 12- and 14-atom clusters and for all the other channels $i=1$, 3, 4, 5, 6, and 7 as well. (An alternative approach is to add the rotational energies to the MEP's, which produces centrifugal barriers; see discussion below.) Thus the fragmentation energies are calculated from the minimum-energy structures of the parent and fragment clusters (see Fig. 3). These fragmentation energies are shown in Fig. 4. The feature to notice is that the energy needed to eject a monomer from $(M)_{12}$ and $(M)_{13}$ is higher than the energies of fragmentation into other channels. In contrast, for $(M)_{14}$ the energy required to evaporate one atom is higher only than the energy of fragmentation into channel $i=2$. In order to calibrate the fragmentation energies one may compare them with the melting energies of the corresponding parent clusters. In distinction from the bulk matter, clusters melt over a range of energies of finite size [19,30]. The values of the energies (in reduced units) limiting the melting range from above (these energies are measured from the bottom of the potential well corresponding to the most stable isomer of each cluster) are $\sim 0.74$ for $(M)_{12}$, $\sim 1.33$ for $(M)_{13}$, and $\sim 1.28$ for $(M)_{14}$. The fragmentation rate constants depend on the energy of the clusters. In order to obtain adequate statistics of the fragmentation processes on the time scale of our simulations we had to consider energies considerably higher than either the fragmentation or the melting energies. Therefore in these simulations the clusters are fragmenting from a fully developed liquidlike state.

We present first some results on the dynamics of the fragmentation process. In Fig. 5 the short-time-averaged kinetic energy of a 13-atom system is shown as a function of time. Two nonoverlapping branches of the graph are clearly distinguishable despite the relatively large fluctuations in them. The large fluctuations are consequences of the liquidlike state of the system. Since the total energy is conserved, the abrupt change from the high-kinetic-energy branch to the low-kinetic-energy branch at $t \approx 2.6 \times 10^4$ steps reflects a rapid increase in the potential energy of the melted $(M)_{13}$. The increase in the potential energy is caused by the fragmentation of the cluster into a dimer and an 11-mer. The time evolution of the short-time-averaged kinetic energy serves, thus, as a sensitive indicator not only of isomerization and meltinglike transitions [19,29,30] in a cluster, but also of its fragmentation.

Complementary information on the process shown in Fig. 5 is presented in Figs. 6 and 7. Figure 6 displays the instantaneous kinetic energy of the relative motion of the $(M)_2$ and $(M)_{11}$ fragments and their instantaneous interaction energy as functions of time. Since the total linear momenta $\mathbf{P}_i$ and $\mathbf{P}_{n-i}$ of the separating fragments may not lie along the line of their c.o.m.'s, the kinetic-energy release is, in general, the sum of the energies of the orbital rotation of the fragments, due to the components $\mathbf{P}_{i\perp}$ and $\mathbf{P}_{n-i\perp}$ perpendicular to the line of the c.o.m.'s, and of their relative translational motion, due to the components $\mathbf{P}_{i\parallel}$ and $\mathbf{P}_{n-1\parallel}$ along the line of the c.o.m.'s (see Fig. 8). The interaction energy shown in Fig. 6 is calculated from configurations generated along a trajectory and should be distinguished from the type of the interaction energy shown in Fig. 1. As the fragments

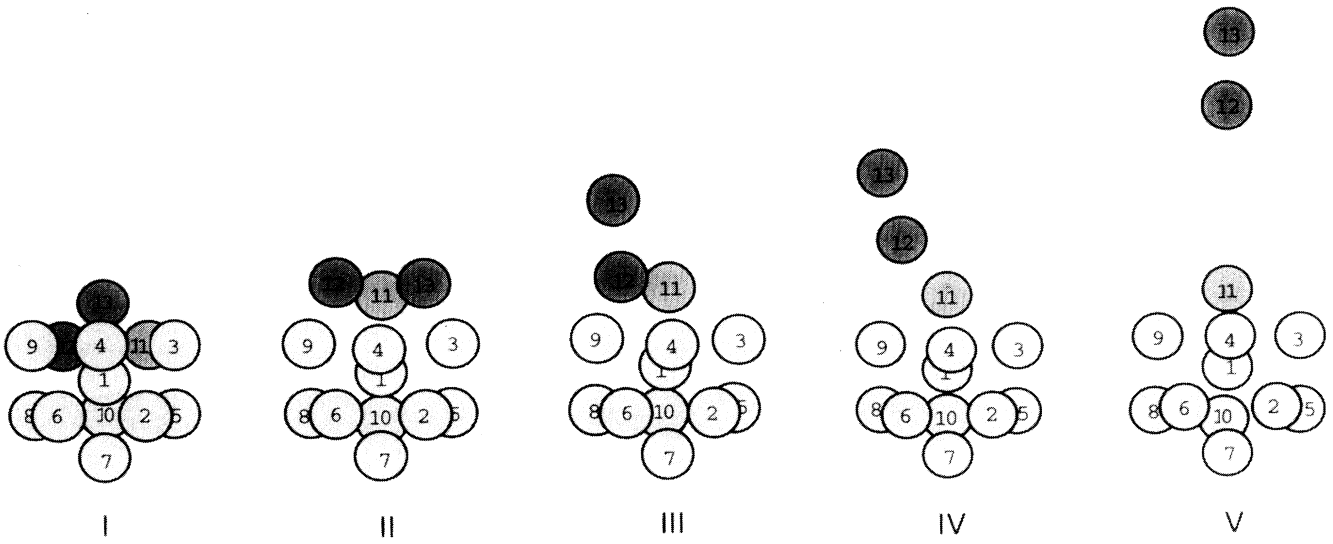


FIG. 2. Minimum-energy configurations of the 13-atom system corresponding to different values of $S^*$. The roman numerals establish the correlation with Fig. 1. Configurations I and II are true minimum-energy isomers.

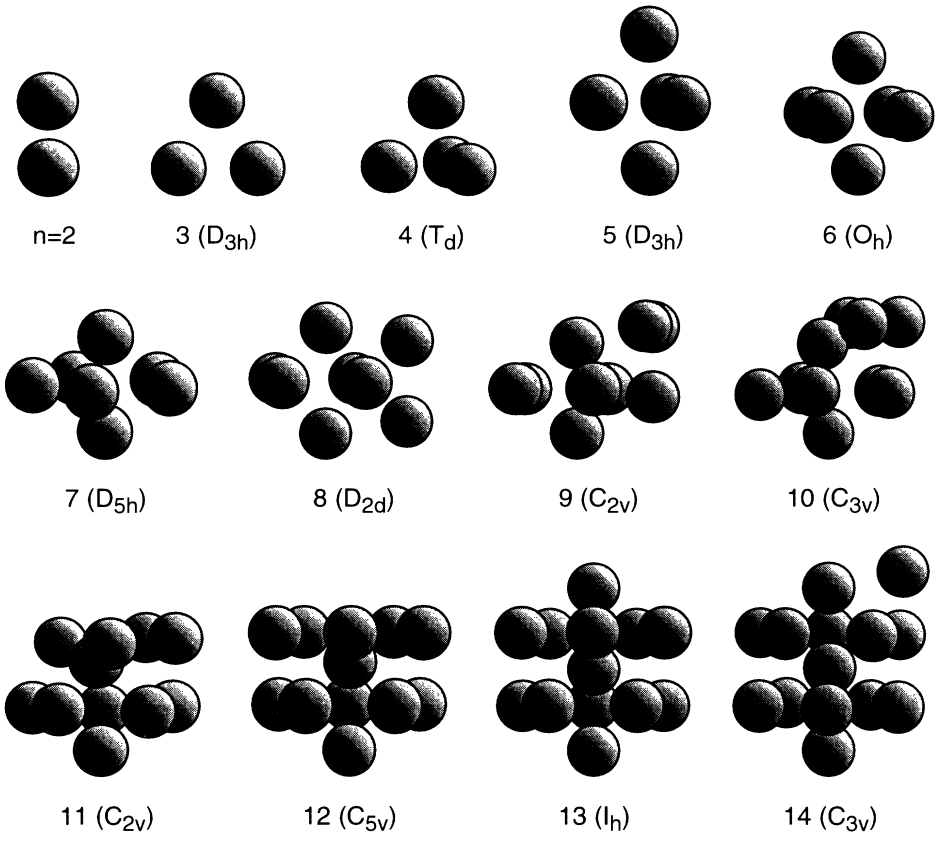


FIG. 3. The most stable structures and their symmetries of the $(M)_n$, $n=2-14$, clusters. The energies of these clusters in reduced units are: $-1.211$, $-2.160$, $-3.187$, $-4.170$, $-5.215$, $-6.209$, $-7.193$, $-8{,}200$, $-9.222$, $-10.234$, $-11.292$, $-12.463$, and $-13.398$, respectively.

separate with time their interaction energy approaches zero. The instant of fragmentation along a given trajectory can be defined as the time at which the absolute value of the interaction energy becomes less than a predefined small positive quantity. As the fragments become free, the kinetic energy of their relative motion becomes constant.

Figure 7 depicts the distance $S$ between the c.o.m.'s of $(M)_2$ and $(M)_{11}$ as a function of time (cf. Fig. 8). As the fragments become free this distance becomes a monotonic function of time. The equation of the segment of the graph corresponding to the free motion of the fragments is

$$S(t)=\left[S_0^2+\frac{2}{\mu}\sqrt{(S_0^2P_0^2-L_0^2)}(t-\tau_0)+\frac{1}{\mu^2}P_0^2(t-\tau_0)^2\right]^{1/2}, \tag{24}$$

where $\tau_0$ is the instant of fragmentation, $S_0=S(t=\tau_0)$, $P_0=P(t=\tau_0)$, and $L_0$ is the magnitude of the constant orbital angular momentum $\mathbf{L}_0$ of the free fragments,

$$\mathbf{L}_0=\mathbf{S}_0\times\mathbf{P}_{i0}\ . \tag{25}$$

In Eq. (25), $\mathbf{S}_0$ is the distance vector from the c.o.m. of the $(n-i)$-atom fragment to the c.o.m. of the $i$-atom fragment at $t=\tau_0$ and $\mathbf{P}_{i0}=\mathbf{P}_i(t=\tau_0)$. In the limit of large times, $S(t)$ is approximated well by a linear function [cf. Fig. (7)]. Obviously, when $L=0$, the entire kinetic-energy release is the kinetic energy of the relative

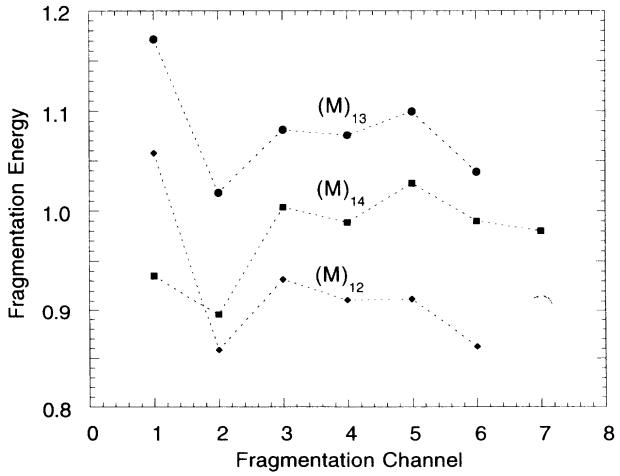


FIG. 4. Fragmentation energies (in reduced units) for $(M)_n$, $n=12-14$.

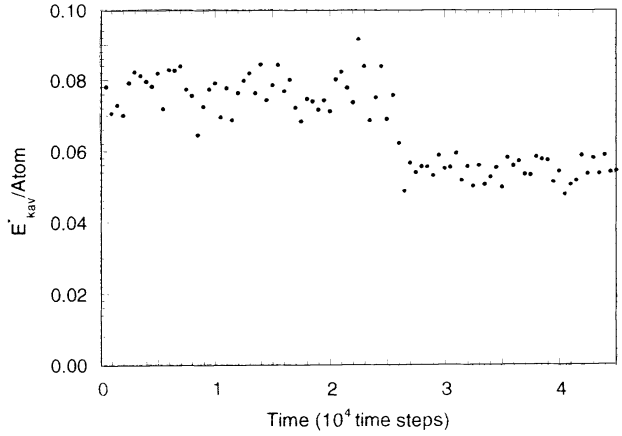


FIG. 5. Short-time-averaged kinetic energy per atom as a function of time for the 13-atom system undergoing fragmentation into a dimer and an 11-mer. The averages are calculated over 500 steps, which corresponds to 3–5 vibrations of the $(M)_{13}$.

translational motion of the fragments and

$$S(t)=S_0+\frac{P_0}{\mu}(t-\tau_0)\ . \tag{26}$$

We emphasize again that at the energy considered the fragmentation of the cluster is a rapid process ($\sim 500$ time steps). The qualitative changes in the graphs of Figs. 5–7 occurring synchronously at $t\approx 2.6\times 10^4$ time steps are all consequences and signatures of this process.

Figure 9 shows the distributions of the fragmentation-channel probabilities for $(M)_n$, $n=12-14$, parent clusters at different total energies per atom. These probabilities are calculated using 200 (for $n=12$ and 14) and 400 (for $n=13$) trajectories per energy. Tests have shown adequate convergence of the results obtained with as few as 200 trajectories. The prominent feature of these distributions is that they peak at channel $i=2$. The evaporation of monomers is practically absent and the probabilities decrease monotonically with $i$ for $i\geq 2$. For the ranges covered, the size and the energy of the clusters seem to have no major effect on the distributions. One can also examine the possible relation between the fragmentation-channel probabilities and the fragmentation energies for a cluster of a given size. The smallest fragmentation energy for $i=2$ correlates with the largest probability of fragmentation into this channel for all the clusters considered. The largest fragmentation energy for $i=1$ in the case of $n=12$ and 13 correlates with the negligibly small values of the corresponding probabilities. However, this latter correlation does not hold for the 14-atom cluster. Similarly to the 12-mer and the 13-mer, the 14-mer prefers not to evaporate atoms despite the fact that its evaporation energy is the second smallest of all its fragmentation energies. The oscillating, as a function of $i$ (for $i\geq 2$), fragmentation energies do not correlate with the monotonic decrease of the corresponding channel probabilities.

One is tempted to compare the probabilities of Fig. 9 with those following from the RRK treatment in spite of the fact that the latter does not include the possible orbital and rotational motions of the fragments. The RRK

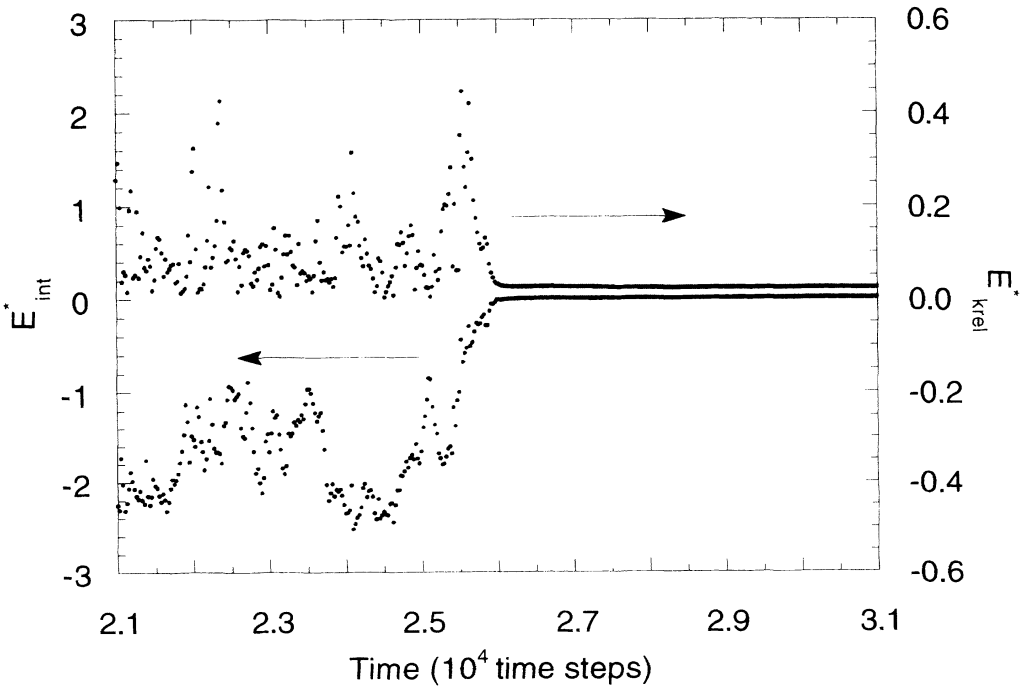


FIG. 6. Interaction energy and kinetic energy of the relative motion of the $(M)_2$ and $(M)_{11}$ fragments as functions of time. Both are calculated for configurations along the same trajectory that generates Fig. 5.

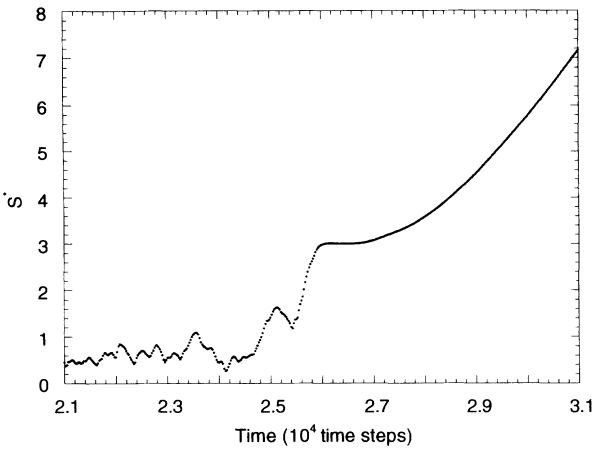


FIG. 7. Distance between the centers of mass of the $(M)_2$ and $(M)_{11}$ fragments as a function of time. The graph is calculated along the same trajectory that generates Figs. 5 and 6.

fragmentation-channel probabilities are calculated using Eqs. (17), (14), and (19) [Eq. (19) defines the channel-specific rate constants] and assuming that the frequency factor $\nu$ is the same for all the channels. The distributions of these probabilities are presented in Fig. 10. For each parent cluster, they are in direct correlation, or rather anticorrelation, with the corresponding fragmentation energies. The monotonic increase of the smaller and decrease of the larger fragmentation-channel probabilities with the increase of the cluster energy reflects the fact that in the limit of very high energies the RRK rate constants, Eq. (19), tend to the same limit for all the fragmentation channels of a given parent cluster. As a consequence, the distribution of the RRK fragmentation-channel probabilities becomes more uniform as the energy of the cluster is increased.

The global fragmentation rate constants are obtained from linear fits of the logarithms of the time-dependent survival probabilities $P(t)$, Eq. (12). These probabilities, as calculated from the dynamical simulations, are shown for the case of the 13-atom parent cluster in Fig. 11. The rate of decay of the survival probabilities is indeed exponential and it increases with the energy of the cluster. Figure 12 displays the global fragmentation rate constants for the 12-, 13-, and 14-atom clusters. As expected (e.g., from the RRK model), the rate constants increase monotonically with the energy of the clusters. When considered as functions of the total energy per atom, the rate constants, at least for the energy range covered, show only a relatively weak dependence on the cluster size, and the 12-mer and the 13-mer emerge as, respectively, the least and the most resistant to fragmentation.

As has been discussed above, in general there is no consistent and systematic correlation between the fragmentation-channel probabilities (and, consequently, the channel-specific fragmentation rate constants), on the one hand, and the corresponding fragmentation energies, on the other, all considered as functions of the fragmentation channel of a cluster of a given size. Next we address the question about the possibility of such a correlation between the fragmentation rate constants and the fragmentation energies considered as functions of the cluster size. In a direct way this question can be answered for the individual fragmentation channels. The fragmentation rate constants for the dominant channel $i=2$ are shown in Fig. 13. When considered as functions of the total energy per atom, they display the same trends as those exhibited by the global rate constants, Fig. 12, and they correlate with the corresponding fragmentation energies in the sense that larger rate constants correspond to smaller fragmentation energies (cf. Fig. 4). In order to carry out a similar analysis for the global fragmentation rate constants one would have to introduce an effective (averaged over the channels) fragmentation energy of a cluster. The same ordering of the fragmentation rate constants as in Figs. 12 and 13 was obtained by Weerasinghe and Amar (WA) in their study of evaporation (single-atom ejection) from 12-, 13-, and 14-atom Lennard-Jones clusters at higher energies [16,17]. Both the dynamical and the phase-space theory calculations of

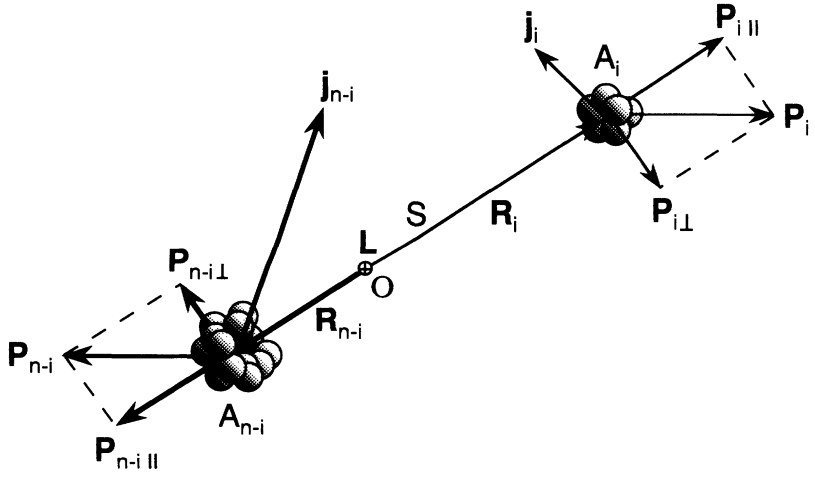


FIG. 8. Schematic of fragmentation of an $n$-atom cluster $(A)_n$ into $(A)_i$ and $(A)_{n-i}$ fragments. **P** stands for the linear momenta, **j** for the rotational angular momenta, and **L** (perpendicular to the plane of the figure) for the orbital angular momentum of the fragments (see text). $O$ is the center of mass of the $n$-atom system, $S=R_i+R_{n-i}$.

WA, however, indicate a crossover between the evaporation rate constants of the 12- and 14-atom clusters as the energy of the clusters is decreased. The low-energy tails of the graphs in Figs. 12 and 13 are also suggestive of the possibility of such a crossover. We will address this point in greater detail in future publications.

It is of interest to compare the dynamical simulation results regarding the dependence of the individual channel-specific rate constants on the size of the parent cluster with the corresponding predictions of the RRK model. It would not be meaningful to consider the RRK channel-specific rate constants for parent clusters of different sizes at the same value of the total energy per atom or per degree of freedom. The reason is that the dependence on the cluster size enters the RRK expression for the rate constant, Eq. (19), not only through the number of the degrees of freedom $s$ but also through the value of the threshold energy $E_0$ and, in princple, that of the frequency factor $\nu$. Assuming that $\nu$ has the same value for the different parent clusters (which is not a severe assumption—see the discussion below) and introducing $\alpha = E/E_0(i|n)$, where $E_0(i|n)$ is the $i$-channel fragmentation energy of an $n$-atom cluster, one can rewrite Eq. (19) in the form

$$k(\alpha) = \nu \left[ 1 - \frac{1}{\alpha} \right]^{s-1}, \tag{27}$$

which retains the dependence on the cluster size only through $s$. In order to compare the dynamical simulation

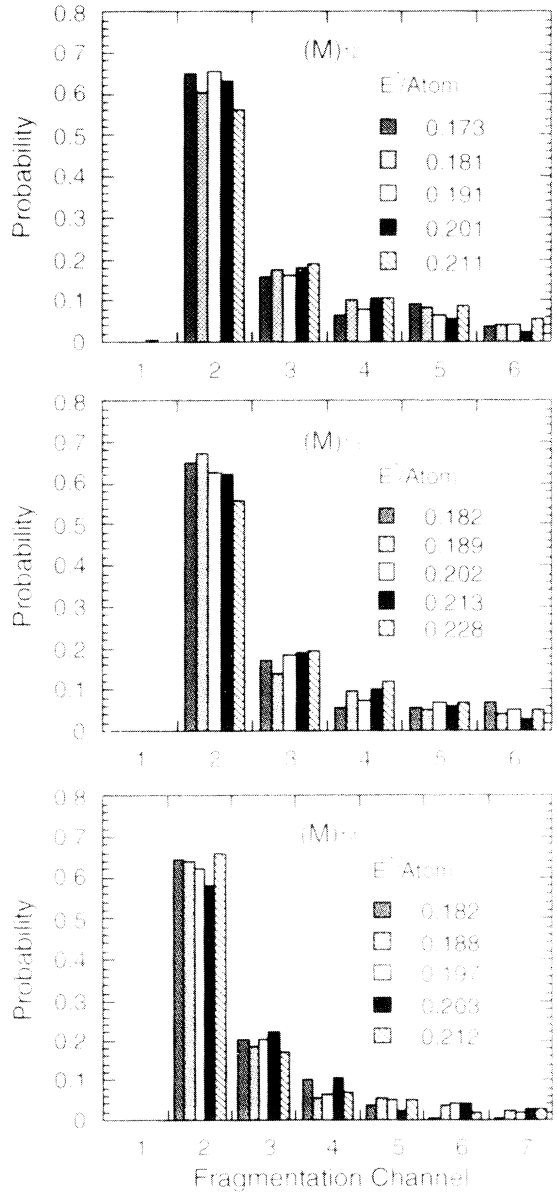


FIG. 9. Fragmentation-channel probabilities calculated from molecular-dynamics simulations for $(M)_n$, $n = 12-14$, clusters at different total energies (per atom). For each cluster the energies are defined with respect to the bottom of the potential-energy well corresponding to its most stable geometry.

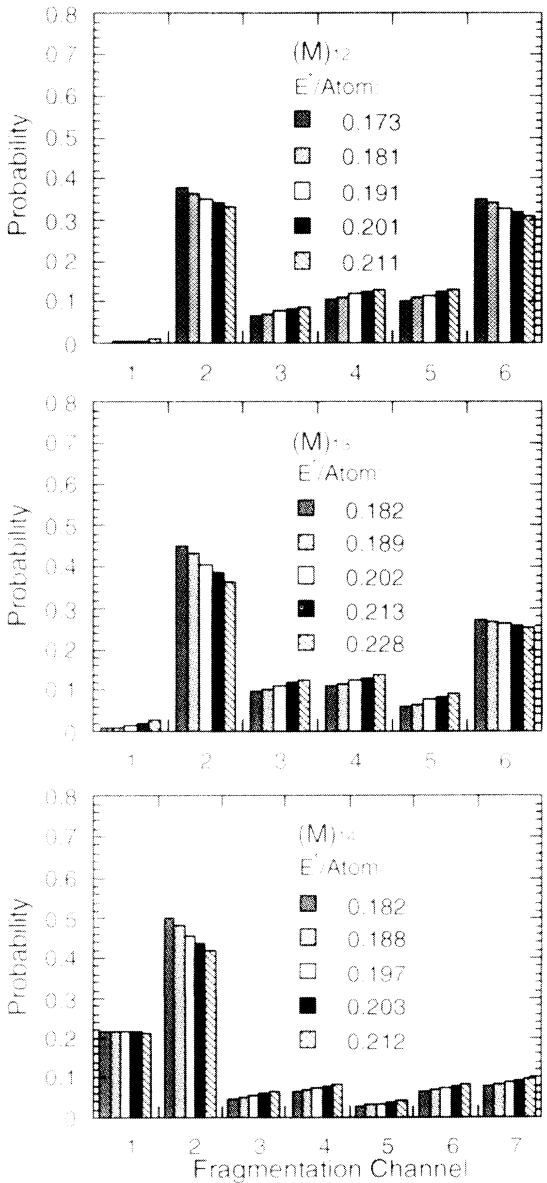


FIG. 10. The same as Fig. 9 but calculated from the RRK model.

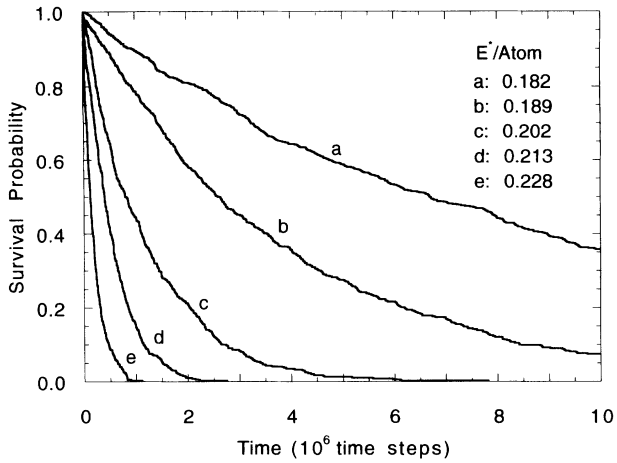


FIG. 11. Survival probability of the $(M)_{13}$ cluster as a function of time. The graphs are obtained from dynamical simulations at the same energies as considered in Fig. 9.

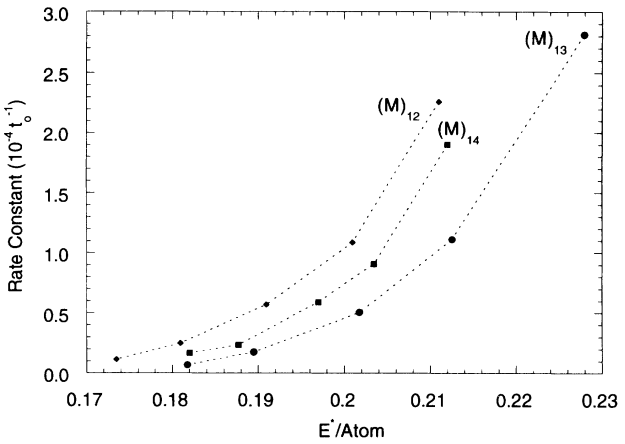


FIG. 13. The same as Fig. 12 but for the channel-specific fragmentation rate constants of the processes $(M)_n \rightarrow (M)_2 + (M)_{n-2}$.

results for the channel-specific rate constants with the corresponding RRK results calculated using Eq. (27) one has to reproduce the former as functions of $\alpha$. The $\alpha$ dependence of the fragmentation rate constants for $i=2$ derived from the dynamical simulations is shown in Fig. 14. One notices the change in the ordering of the rate constants for the different parent clusters as compared to that in Fig. 13. Our main goal, however, is to answer the question: Does the ordering in Fig. 14 coincide with the one following from the RRK model calculations? The answer to this question is "no," at least for the range of $\alpha$'s covered by the dynamical simulations. This is evident from the inspection of Fig. 15, which displays the RRK results obtained using Eq. (27) with $\nu=0.9t_0^{-1}$. This choice of the value of $\nu$ is based on the following consideration. For metals the frequency of the diatomic molecule and the corresponding Debye frequency of the bulk are not very different. For example, for nickel they are $0.99\times10^{13}$ and $0.94\times10^{13}$ Hz, respectively [46,47]. Since the rate constants are indeed insensitive to small variations in the frequencies, one can assign a single characteristic frequency to a metal system irrespective of its size. Our choice of the value of $\nu$ is based on the magnitude $0.94t_0^{-1}$ of the Debye frequency of nickel, where $t_0$, Eq. (4), is calculated using $U=3.77$ eV, appropriate for bulk nickel.

Finally, in Fig. 16 we compare the rate constants for the fragmentation of a 13-mer into a dimer and an 11-mer obtained using dynamical simulations with those of the RRK and TST approacnes. The TST results are calculated applying Eqs. (20)–(22). The transition state is chosen at the separation $3.36r_0$ of the fragments at which the interaction energy between the dimer and the 11-mer, as calculated from their $S$-constrained minimum energy structures, becomes smaller than 0.001 (reduced units). Based on the consideration discussed above, the same value $0.9t_0^{-1}$ is assigned to all the frequencies $\nu_i$ and $\nu_i^{\dagger}$. Although the 11-atom fragment is liquidlike at the ener-

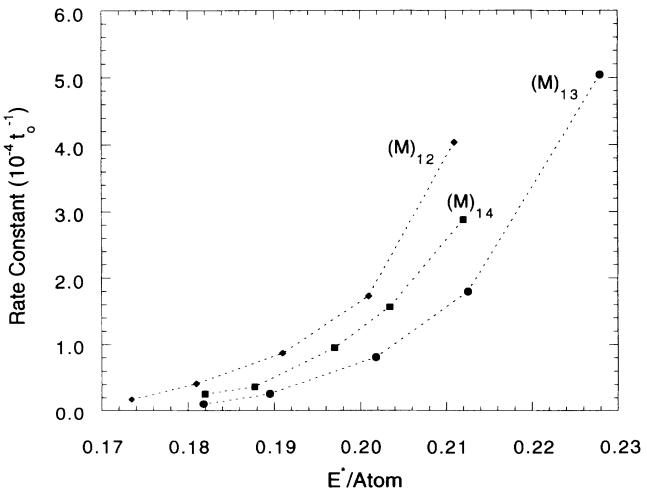


FIG. 12. Microcanonical global fragmentation rate constants for $(M)_n$, $n=12$–14, parent clusters as functions of the cluster energy per atom. The graphs are obtained from dynamical simulations. The energies are defined as explained in the caption of Fig. 9. The unit $t_0$ of time is defined by Eq. (4).

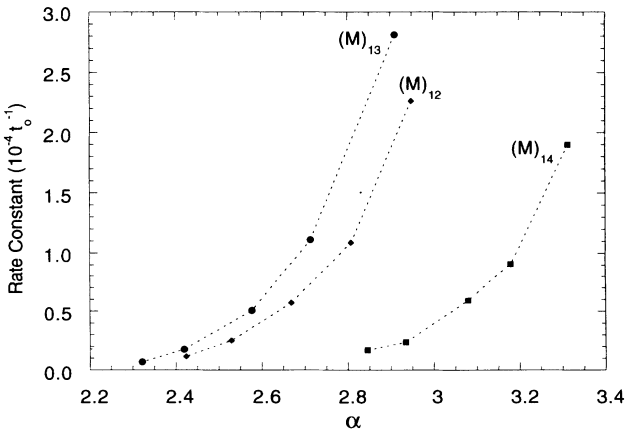


FIG. 14. The same as Fig. 13 but plotted as a function of $\alpha$ (see text).

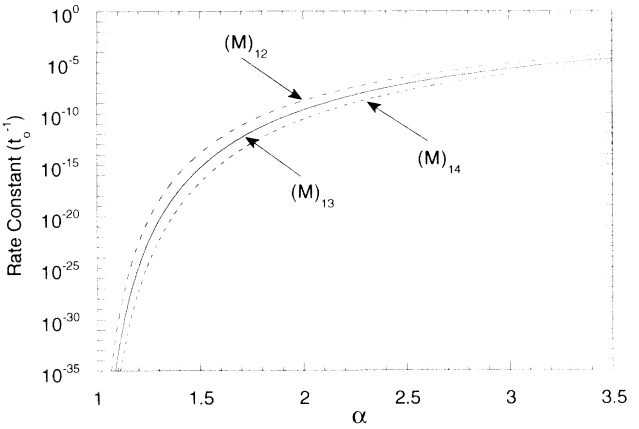


FIG. 15. The same as Fig. 14 but calculated from the RRK model. Notice the difference in the range of $\alpha$ as compared to that in Fig. 14.

gies considered, its (time-)averaged structure is assumed to be a spherical top. Taking into account that the effective sizes of the 11- and 13-atom clusters are very close, we obtain the moment of inertia $I_1$ of the $(M)_{11}$ fragment from that of the equilibrium icosahedral structure of $(M)_{13}$ by rescaling the mass. The moment of inertia $I_2$ of the dimer is calculated at its equilibrium interatomic distance. The symmetry number of the dimer is 2 and those of the 11-mer and the 13-mer are 11! and 13!, respectively, since these clusters are liquidlike [48]. Because the moment of inertia $I_0$ of the orbital motion is considerably larger than $I_1$ and $I_2$, $W^{\dagger}(E,J=0)$, Eq. (21), and, consequently, the TST rate constant are only weakly sensitive to the precise value of $I_0$, which, in turn, depends on the choice of the position of the transition state.

It is quite remarkable that over the energy range considered the different approaches give approximately the same rate of change of the rate constant with the energy.

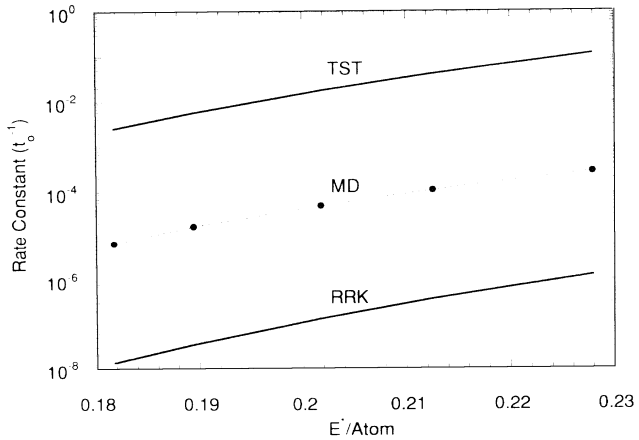


FIG. 16. Microcanonical channel-specific rate constants for the process $(M)_{13} \rightarrow (M)_2 + (M)_{11}$ calculated from dynamical simulations (MD) and the RRK and TST statistical approaches. The energies are defined as explained in the caption of Fig. 9.

The TST values are larger than those derived from the dynamics, which is consistent with the fact that the TST defines an upper limit for the rate constants. Replacing the harmonic densities of states for the parent cluster and the fragments by the more adequate anharmonic densities would most probably lead to lower values of the TST rate constant. The reason is that the anharmonic density increases with energy faster than the harmonic one [17] and it is reasonable to expect that the difference between the two is larger for a system with a larger number of degrees of freedom. Thus replacing the harmonic densities of states by the anharmonic ones would result in a larger increment of the density of states for the parent cluster than for the fragments. The effect could further be magnified by that the internal energy at which one evaluates the densities of states is higher for the parent cluster than for the fragments.

The values of the RRK rate constant calculated assuming $s=3n-6$ are lower than the corresponding values obtained from the dynamics. Again, it is consistent with the common experience that the RRK model underestimates the rate constants unless one introduces an effective number of ("active") degrees of freedom which is smaller than the actual one. The fit of the RRK formula, Eq. (19), with $\nu=0.9t_0^{-1}$ and $E_0^*(2|13)=1.02$ (reduced units) to the values of the rate constant obtained from the dynamical simulations yields $s \approx 19$.

The metal clusters are mimicked in this study by a model potential. Since we express this potential in reduced units of energy and distance, the results yield qualitative and relative, rather than absolute, quantitative information. In order to convert the results into absolute quantities one would have to have a single value of the "unit of energy" $U$ appropriate for the cluster and fragment sizes considered. The original parametrization of the potential, Eq. (2), does not provide for this. (An approximate estimate of the order of magnitude of the physical quantities in the absolute units can be obtained using the above-mentioned values of $U$ and $\nu$ appropriate for bulk nickel.) We are currently examining alternative parametrizations.

The emphasis in this study is on the qualitative features of the dynamics of cluster fragmentation, as defined by the model potential used, and on the comparison of the results obtained from the dynamical simulations with the implications of the statistical models. The general conclusion one derives from this comparison is that although there seems to be a partial agreement between the results of the two approaches, this agreement is not a systematic and consistent one. It is not only the energetic characteristics, as implied by the RRK model, or the energetic and entropic (density of states) characteristics, as defined by the TST approach, but also the dynamical factors that affect and govern the phenomenon of cluster fragmentation.

The results of both, the dynamical and the statistical, treatments depend on the built-in (explicitly or implicitly) approximations and/or assumptions. One of the approximations built into the dynamical simulations is the potential energy function chosen to mimic the cluster cohesion. An important question in this respect is how sensitive are

the results to the parameters of the potential. We will address this question in future publications. Here we note only that some of the results, for example, the pattern of the fragmentation channel probabilities, may, in fact, be quite sensitive. It is the comparison of the theoretical predictions with the appropriate experimental data, when available, which will ultimately allow for "tuning" of the cluster potentials. Theoretical studies of the cluster fragmentation yield information on the implications of a chosen potential that is complementary to that extracted from the investigation of the structural forms of and phases and phase changes in these systems.

An assumption used in the TST treatment is the location of the transition state. An alternative to the approach used in this study is to add the rotational energies to the MEP and to place the transition state at the position of the effective barrier, provided such a barrier exists (we are currently exploring this option). A change in the position of the transition state will, in general, change the value of the threshold energy $E_0$, which in turn may, and usually will, affect the rate constants.

## V. SUMMARY

In this study we describe dynamical and statistical approaches to multichannel fragmentation of atomic clusters. These approaches are applied to model metal clusters. The fragmentation phenomenon, as a function of the cluster size and energy, is characterized in terms of fragmentation-channel probabilities and rate constants (global and channel-specific). The comparison of the results obtained from the dynamical simulations with those following from the statistical models indicates that dynamical effects may play an important role in cluster fragmentation. The analysis of the distribution of the available energy between the fragments will be given separately. Future presentations will also examine the question about the sensitivity of the results described here to the details of the potential-energy surface chosen to model the interatomic interactions in a cluster.

## ACKNOWLEDGMENTS

We thank Dr. M. Knickelbein for stimulating discussions and Dr. M. Trache for a useful exchange during a conference in Elounda, Crete. This work was performed under the auspices of the Office of Basic Energy Sciences, Division of Chemical Science, U.S. DOE, under Contract No. W-31-109-ENG-38. M.J.L. would like to acknowledge financial support through a Fulbright-MEC grant.

[1] T. D. Märk, Int. J. Mass Spectrom. Ion Phys. **79**, 1 (1987); J. E. Campana, Mass Spectrom. Rev. **6**, 395 (1987).
[2] J. R. Heath, Y. Lin, S. C. O'Brien, Q.-L. Zhang, R. F. Curl, F. K. Tittel, and R. E. Smalley, J. Chem. Phys. **83**, 5520 (1985).
[3] M. J. Jarrold, J. E. Bower, and J. S. Kraus, J. Chem. Phys. **86**, 3876 (1987).
[4] A. J. Stace, J. Chem. Phys. **85**, 5774 (1986).
[5] P. J. Brucat, L.-S. Zheng, C. L. Pettiette, S. Yang, and R. E. Smalley, J. Chem. Phys. **84**, 3078 (1986).
[6] C. Bréchignac, Ph. Cahuzac, J. Leygnier, and J. Weiner, J. Chem. Phys. **90**, 1492 (1989).
[7] M. E. Gusic, M. F. Jarrold, J. L. McIlrath, R. R. Freedman, and W. L. Brown, J. Chem. Phys. **86**, 3862 (1987).
[8] U. Ray, M. F. Jarrold, J. E. Wower, and J. S. Kraus, J. Chem. Phys. **91**, 2912 (1989).
[9] L. Lian, C.-X. Su, and P. B. Armentrout, J. Chem. Phys. **96**, 7542 (1992); P. B. Armentrout, D. H. Hales, and L. Lian, in *Advances in Metal and Semiconductor Clusters,* edited by M. Duncan (JAI Press, Greenwich, in press), Vol. II.
[10] O. K. Rice and H. C. Ramsperger, J. Am. Chem. Soc. **49**, 1617 (1982); S. L. Kassel, J. Chem. Phys. **32**, 225 (1928); **32**, 1065 (1928).
[11] R. A. Marcus and O. K. Rice, J. Phys. Colloid Chem. **55**, 894 (1951); R. A. Marcus, J. Chem. Phys. **20**, 359 (1952); G. M. Wieder and R. A. Marcus, *ibid.* **37**, 1835 (1962); R. A. Marcus, *ibid.* **43**, 2658 (1965).
[12] W. Forst, *Theory of Unimolecular Reactions* (Academic, New York, 1973).
[13] R. G. Gilbert and S. C. Smith, *Theory of Unimolecular and Recombination Reactions* (Blackwell Scientific, Oxford, 1990).
[14] S. C. Smith, J. Chem. Phys. **95**, 3404 (1991); **97**, 2406 (1992).
[15] M. F. Jarrold, in *Clusters of Atoms and Molecules,* edited by H. Haberland, Springer Series in Chemical Physics Vol. 52 (Springer-Verlag, Berlin, in press).
[16] F. G. Amar and S. Weerasinghe, in *Mode Selective Chemistry,* edited by J. Jortner, R. D. Levine, and B. Pullman (Kluwer Academic, Dordrecht, 1991), p. 165.
[17] S. Weerasinghe and F. G. Amar, J. Chem. Phys. **98**, 4967 (1993).
[18] C. L. Briant and J. J. Burton, J. Chem. Phys. **63**, 2045 (1975).
[19] J. Jellinek, T. L.Beck, and R. S. Berry, J. Chem. Phys. **84**, 2783 (1986); H. L. Davis, J. Jellinek, and R. S. Berry, *ibid* **86**, 6456 (1987).
[20] F. G. Amar and R. S. Berry, J. Chem. Phys. **85**, 5943 (1986).
[21] J. D. Honeycutt and H. C. Anderson, J. Phys. Chem. **91**, 4950 (1987).
[22] E. Blaisten-Barojas and D. Levesque, in *Physics and Chemistry of Small Clusters,* edited by P. Jena, B. K. Rao, and S. N. Khanna (Plenum, New York, 1987), p. 157.
[23] J. Luo, U. Landman, and J. Jortner, in *Physics and Chemistry of Small Clusters* (Ref. [22]), p. 201.
[24] A. Heidenreich, J. Jortner, and I. Oref, J. Chem. Phys. **97**, 197 (1992); A. Heidenreich, I. Schek, D. Scharf, and J. Jortner, Z. Phys. D **20**, 227 (1991).
[25] J. Rose and R. S. Berry, J. Chem. Phys. **96**, 517 (1992); Z. Phys. D **26**, 178 (1993); **26**, 189 (1993).
[26] S. Sawada and S. Sugano, Z. Phys. D. **14**, 247 (1989).
[27] U. Röthlisberger and W. Andreoni, J. Chem. Phys. **94**,

[28] F. Ercolessi, W. Andreoni, and E. Tossatti, Phys. Rev. Lett. **66**, 911 (1991).

[29] Z. B. Güvenç, J. Jellinek, and A. F. Voter, in *Physics and Chemistry of Finite Systems: From Clusters to Crystals*, edited by P. Jena, S. N. Khanna, and B. K. Rao (Kluwer Academic, Dordrecht, 1992), Vol. I, p. 411; Z. B. Güvenç and J. Jellinek, Z. Phys. D **26**, 304 (1993).

[30] I. L.Garzón and J. Jellinek, Z. Phys. D **20**, 235 (1991); J. Jellinek and I. L. Garzón, *ibid.* **20**, 239 (1991); I. L.Garzón and J. Jellinek, in *Physics and Chemistry of Finite Systems: From Clusters to Crystals* (Ref. [29]), Vol. I, p. 405; Z. Phys. D **26**, 316 (1993). All values of the kinetic energy and of the temperature reported in these references have to be divided by 2. The validity of the qualitative conclusions remains unaffected.

[31] M. S. Stave and A. E. DePristo, J. Chem. Phys. **97**, 3386 (1992); K. Raghavan, M. S. Stave, and A. E. DePristo, *ibid.* **91**, 1904 (1989).

[32] J. Uppenbrink and D. Wales, J. Chem. Phys. **96**, 8521 (1992); Z. Phys. D **26**, 258 (1993).

[33] R. N. Barnett, U. Landman, and G. Rajagopal, Phys. Rev. Lett. **67**, 3058 (1991).

[34] J. M. Soler, J. J. Saez, N. Garcia, and O. Echt, Chem. Phys. Lett. **109**, 71 (1984); J. J. Saez, J. M. Solder, and N. Garcia, Surf. Sci. **156**, 121 (1985).

[35] R. W. Smith, Z. Phys. D **21**, 57 (1991);

[36] C. E. Román and I. L. Garzón, Z. Phys. D **20**, 263 (1991); in *Physics and Chemistry of Finite Systems: From Clusters in Crystals* (Ref. [29]), Vol. I, p. 459.

[37] C. Rey, L. J. Gallego, M. P Iñiguez, and J. A. Alonso, Physica B **179**, 273 (1992).

[38] D. H. Gross, Rep. Prog. Phys. **53**, 605 (1990).

[39] X. Campi, in *The Chemical Physics of Atomic and Molecular Clusters*, edited by G. Scoles (Elsevier, Amsterdam, 1990), p. 237.

[40] C. E. Klots, J. Chem. Phys. **83**, 5854 (1985); Z. Phys. D **5**, 83 (1987).

[41] J. J. Saez, J. M. Soler, and N. Garcia, Chem. Phys. Lett. **114**, 15 (1985).

[42] R. P. Gupta, Phys. Rev. B **23**, 6265 (1981).

[43] F. Ducastelle, J. Phys. (Paris) **31**, 1055 (1970).

[44] L. Verlet, Phys. Rev. **159**, 98 (1967); W. C. Swope and H. C. Andersen, J. Chem. Phys. **76**, 637 (1982).

[45] D. G. Truhlar, W. L. Hase, and J. T. Hynes, J. Phys. Chem. **87**, 2664 (1983).

[46] M. D. Morse, Chem. Rev. **86**, 1049 (1986).

[47] C. Kittel, *Introduction to Solid State Physics* (Wiley, New York, 1966).

[48] R. S. Berry, J. Jellinek, and G. Natanson, Phys Rev. A **30**, 919 (1984); G. Natanson, F. Amar, and R. S. Berry, J. Chem. Phys. **78**, 399 (1983).

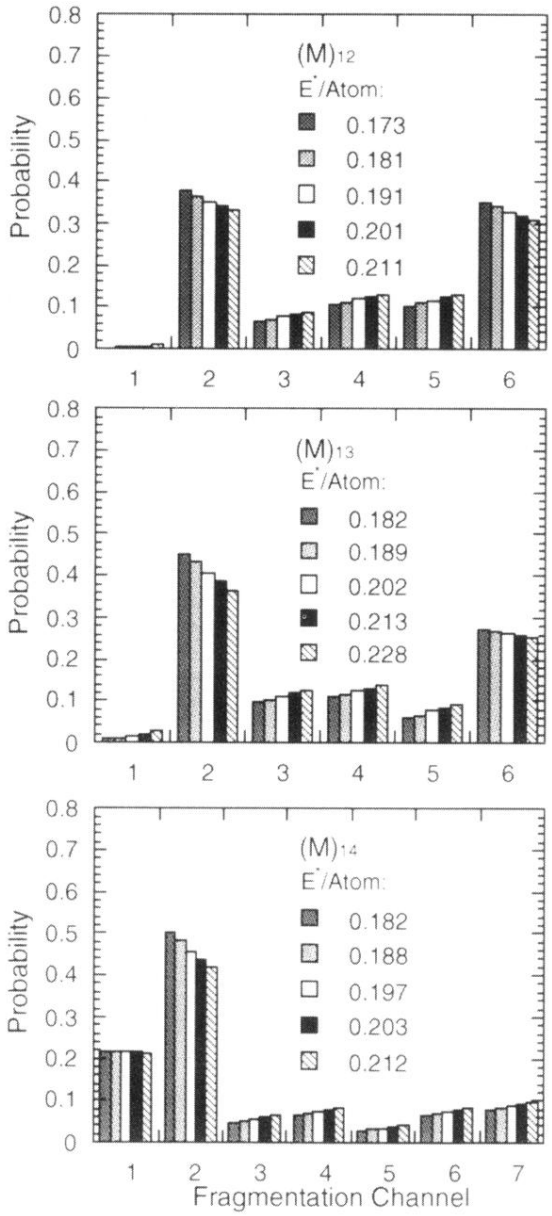


FIG. 10. The same as Fig. 9 but calculated from the RRK model.

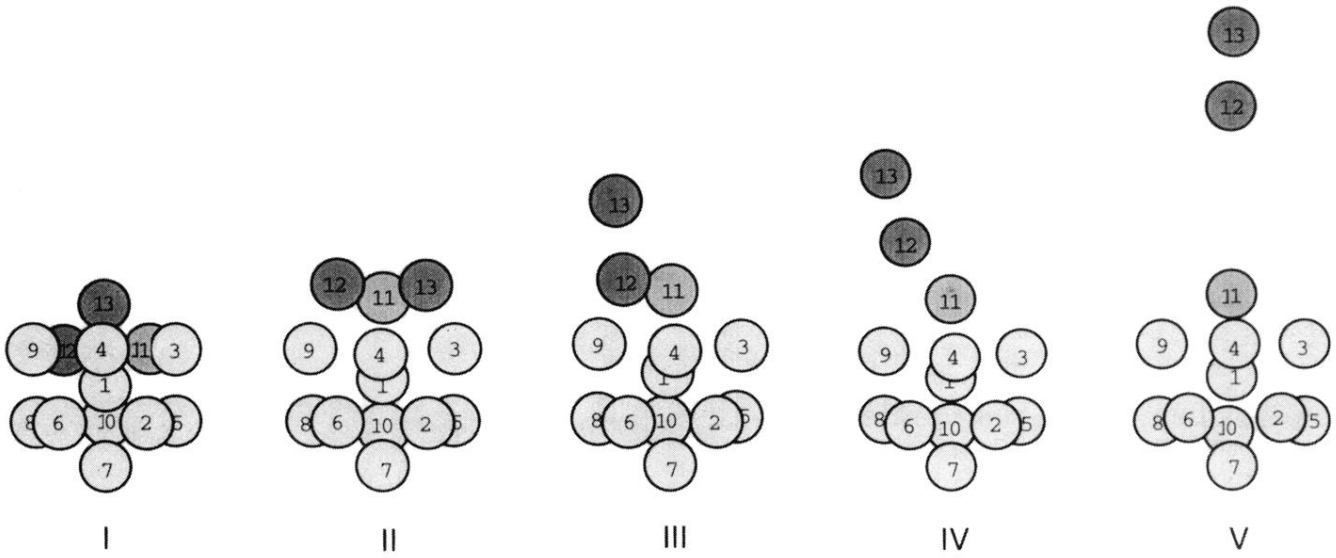


FIG. 2. Minimum-energy configurations of the 13-atom system corresponding to different values of $S^*$. The roman numerals establish the correlation with Fig. 1. Configurations I and II are true minimum-energy isomers.

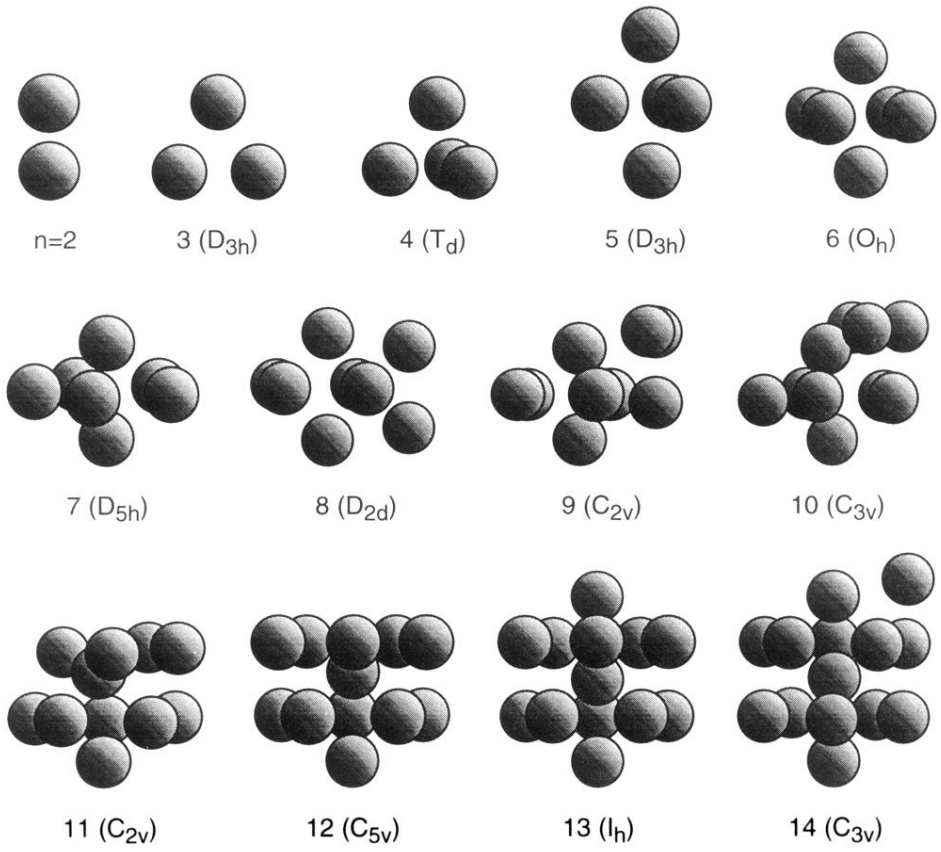


FIG. 3. The most stable structures and their symmetries of the $(M)_n$, $n=2-14$, clusters. The energies of these clusters in reduced units are: $-1.211$, $-2.160$, $-3.187$, $-4.170$, $-5.215$, $-6.209$, $-7.193$, $-8{,}200$, $-9.222$, $-10.234$, $-11.292$, $-12.463$, and $-13.398$, respectively.

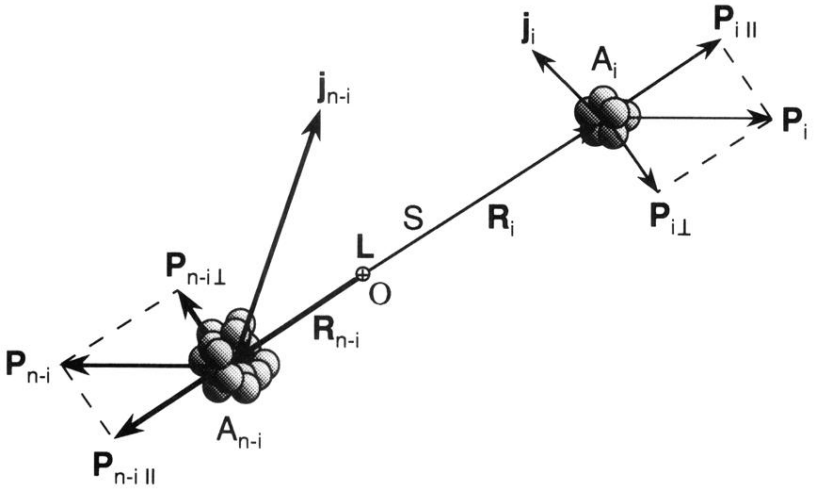


FIG. 8. Schematic of fragmentation of an $n$-atom cluster $(A)_n$ into $(A)_i$ and $(A)_{n-i}$ fragments. **P** stands for the linear momenta, **j** for the rotational angular momenta, and **L** (perpendicular to the plane of the figure) for the orbital angular momentum of the fragments (see text). $O$ is the center of mass of the $n$-atom system, $S = R_i + R_{n-i}$.

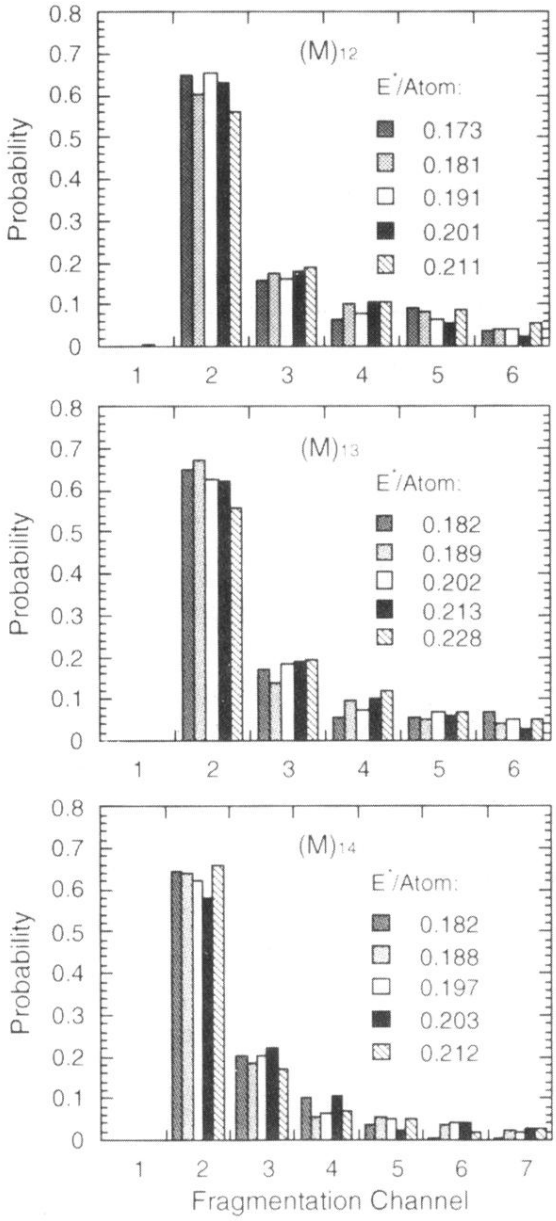


FIG. 9. Fragmentation-channel probabilities calculated from molecular-dynamics simulations for $(M)_n$, $n=12-14$, clusters at different total energies (per atom). For each cluster the energies are defined with respect to the bottom of the potential-energy well corresponding to its most stable geometry.